Topological metallic phases in spin–orbit coupled bilayer systems

2014 New J. Phys. 16 123015

(http://iopscience.iop.org/1367-2630/16/12/123015)

New Journal of Physics
The open access journal at the forefront of physics
Deutsche Physikalische Gesellschaft DPG | IOP Institute of Physics

Topological metallic phases in spin–orbit coupled bilayer systems

Hui Pan[1], Xin Li[1], Zhenhua Qiao[2,3], Cheng-Cheng Liu[4], Yugui Yao[4] and Shengyuan A Yang[5]

[1] Department of Physics, Beihang University, Beijing 100191, People's Republic of China
[2] Department of Physics, University of Science and Technology of China, Hefei, Anhui 230026, People's Republic of China
[3] ICQD, Hefei National Laboratory for Physical Sciences at Microscale, University of Science and Technology of China, Hefei, Anhui 230026, People's Republic of China
[4] School of Physics, Beijing Institute of Technology, Beijing 100081, People's Republic of China
[5] Engineering Product Development, Singapore University of Technology and Design, Singapore 138682, Singapore
E-mail: hpan@buaa.edu.cn and shengyuan_yang@sutd.edu.sg

Received 25 August 2014, revised 16 October 2014
Accepted for publication 23 October 2014
Published 8 December 2014
New Journal of Physics **16** (2014) 123015
doi:10.1088/1367-2630/16/12/123015

Abstract

We investigate the influence of different spin–orbit couplings on topological phase transitions in the bilayer Kane–Mele model. We find that the competition between intrinsic spin–orbit coupling and Rashba spin–orbit coupling can lead to two dimensional topological metallic states with nontrivial topology. Such phases, although having a metallic bulk, still possess edge states with well defined topological invariants. Specifically, we show that with preserved time reversal symmetry the system can exhibit a $\mathbb{Z}_2$-metallic phase with spin helical edge states and a nontrivial $\mathbb{Z}_2$ invariant. When time reversal symmetry is broken, a Chern metallic phase could appear with chiral edge states and a nontrivial Chern invariant.

Keywords: topological metallic states, Kane–Mele model, spin-orbit couplings

1. Introduction

Study of the effects of spin–orbit coupling (SOC) has been a central theme in condensed matter physics in the past decade. SOC is an essential ingredient in spintronics, which aims to utilize the electron's spin degree of freedom instead of charge for information processing, with the advantages of smaller size, fast speed and low dissipation. A perhaps more surprising discovery is that SOC can give rise to new quantum states of matter, e.g. topological insulators that are bulk insulators characterized by nontrivial topological invariants and gapless surface (or edge) states. In two dimensions (2D), a topological insulator with time reversal symmetry is also known as the quantum spin Hall (QSH) insulator [1, 2]. It has an insulating bulk and gapless spin helical edge states protected by a topological $\mathbb{Z}_2$ invariant. When time reversal symmetry is broken, the system may realize a quantum anomalous Hall (QAH) [3–7] insulator with chiral edge states protected by a so-called TKNN or Chern invariant [8, 9]. Their intriguing properties have been a subject of intensive investigations in recent years. Experimentally, the QSH effect has been demonstrated in HgTe/CdTe quantum wells [10, 11] and inverted InAs/GaSb quantum wells [12–14], and the QAH effect has been demonstrated in Cr-doped $(Bi,Sb)_2Te_3$ thin films recently [15]. These discoveries further stimulate significant interest in searching for new topological states of matter.

In solid state systems, SOC enters the Hamiltonian in different forms due to different physical origins. For example, in III–V semiconductor quantum wells, there is Dresselhaus SOC from bulk crystalline inversion symmetry breaking, and there also exists Rashba SOC from structural inversion symmetry breaking along the growth direction. The ability to tune the strength of each individual SOC and control their competition is at the heart of spintronics applications. In the seminal work by Kane and Mele that proposed the 2D $\mathbb{Z}_2$ topological insulator, two types of SOC were considered: the intrinsic SOC and the Rashba SOC [16]. It has been shown that the intrinsic SOC favors the QSH state while the Rashba SOC tends to destroy it. Hence their competition determines the topological phase transitions and the phase boundaries between the topologically trivial and nontrivial insulating states.

The Kane–Mele model was first proposed for graphene. Later studies showed that the magnitude of intrinsic SOC in graphene is too small for the QSH effect to be detected experimentally [17–19]. Recently, many new 2D materials have been discovered with enhanced intrinsic type SOC, such as silicene and germanene [20–25], which are group IV counterparts of graphene and 2D honeycomb Bi/Sb halides and hydrides. The strength of intrinsic SOC can be as large as 0.6 eV, as in some Bi halides [26, 27]. This provides promising systems to realize the Kane–Mele model and the QSH effect at room temperature.

In the study of 2D physics, bilayer systems have attracted a lot of interest. Compared with single layer systems, the extra layer degree of freedom can lead to many new physical phenomena and is usually easier to control in practice [28–31]. Furthermore, in terms of topological properties, bilayer systems can differ qualitatively from single layer systems. For example, when two single layers of QSH insulator are combined to form a bilayer system, its $\mathbb{Z}_2$ invariant vanishes and the system becomes topologically trivial. However, when the layer potential U is finite, a topological state with nontrivial topological invariant can appear [32–34]. As another example, it has been found that the Rashba SOC, which tends to destroy the QSH phase in a single layer turns out to favor the QSH phase in bilayer graphene [35]. All these facts indicate that the physics of a bilayer is quite different from the single layer case.

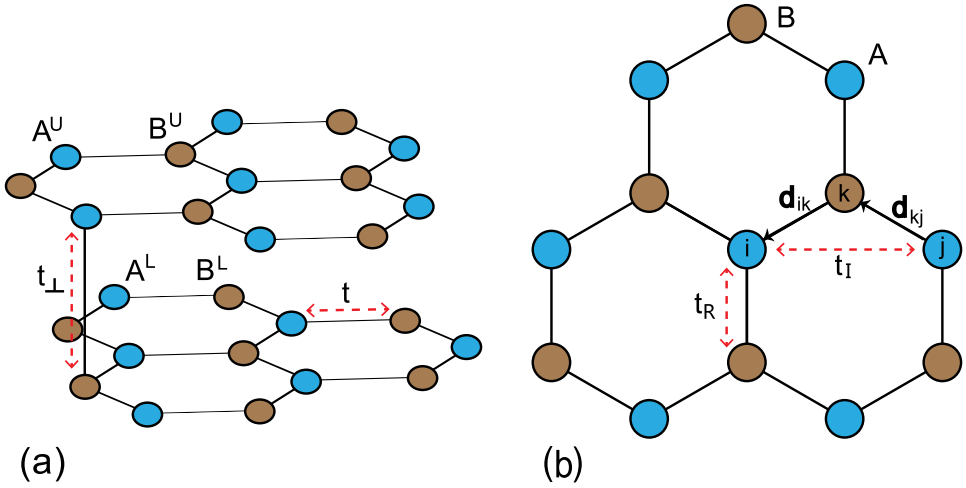

Figure 1. (a) Structure of the bilayer model with the intralayer (interlayer) hopping parameter t ($t_\perp$). The A (B) sublattices are indicated by blue (brown) spheres. (b) Top view of a single layer. d_{ik} and d_{kj} are the nearest-neighbor vectors. $t_{\rm I}$ and $t_{\rm R}$ are respectively intrinsic SOC and Rahsba SOC strengths.

In this work, motivated by the above mentioned progress, we study the effects of different SOCs in a bilayer Kane–Mele model, focusing on its topological properties. We find that the bilayer system exhibits a very rich phase diagram. Quite interestingly, we discover novel 2D topological metallic phases in this system due to the competition between the intrinsic SOC and the Rashba SOC: the 2D $\mathbb{Z}_2$-metallic phase and the Chern metallic phase, depending on whether time reversal symmetry is broken. In such phases, the bulk band gap is closed indirectly, hence a topological invariant can still be well defined, and the state is adiabatically connected to a topologically nontrivial insulator. Like topological insulating phases, the hallmark of the topological metallic phase is the presence of edge states determined by the bulk topology. For the $\mathbb{Z}_2$-metallic phase they are the spin helical edge states, while for the Chern metallic phase they are the chiral edge states. These findings not only extend our understanding of topological states of matter but also may find useful applications based on topological materials.

Our paper is organized as follows. In section 2, we describe the bilayer Kane–Mele model that we study. In section 3, we investigate the case with preserved time reversal symmetry and show that a metallic phase with well defined $\mathbb{Z}_2$ invariant and spin helical edge states can be realized. Section 4 is for the case with time reversal symmetry breaking and we show that there exists a metallic phase with well defined Chern invariant and chiral edge states. Finally, a summary of our work is given in section 5.

2. Physical model

The original Kane–Mele model is written for graphene, which has a honeycomb lattice with one orbital per site and two sites per unit cell. For our bilayer model, we take two AB-stacked honeycomb lattices, each described by a Kane–Mele model, as shown in figure 1. The total Hamiltonian of the system can be written as

$$\mathcal{H} = H^{\mathrm{U}} + H^{\mathrm{L}} + t_{\perp} \sum_{i\in(\mathrm{U,A}),j\in(\mathrm{L,B}),\alpha} \left(c_{i\alpha}^{\dagger} c_{j\alpha} + \mathrm{h.c.} \right) + U \left(\sum_{i\in\mathrm{U},\alpha} c_{i\alpha}^{\dagger} c_{i\alpha} - \sum_{i\in\mathrm{L},\alpha} c_{i\alpha}^{\dagger} c_{i\alpha} \right), \tag{1}$$

where H^{U} and H^{L} are the Hamiltonians for the upper layer and lower layer respectively. The third term is the interlayer coupling. Here, due to the stacking geometry, we only consider the hopping between the A site of the upper layer and the nearest B site of the lower layer. $t_{\perp}$ is the interlayer hopping amplitude. c ($c^{\dagger}$) is the annihilation (creation) operator for an electron, and h. c. denotes the Hermitian conjugate. Subscripts i, j label the lattice sites and α is the spin index. The last term represents an interlayer bias potential with strength U. Each single-layer Hamiltonian $H^{\mathrm{U(L)}}$ is a Kane–Mele model containing the following terms:

$$H^{\mathrm{U(L)}} = H_{\mathrm{hop}} + H_{\mathrm{ISO}} + H_{\mathrm{RSO}} + H_{\mathrm{m}}, \tag{2}$$

where

$$\begin{aligned} H_{\mathrm{hop}} &= -t \sum_{\langle ij\rangle,\alpha} c_{i\alpha}^{\dagger} c_{j\alpha}, \\ H_{\mathrm{ISO}} &= i t_{\mathrm{I}} \sum_{\langle\langle ij\rangle\rangle,\alpha\beta} \nu_{ij} c_{i\alpha}^{\dagger} \sigma_{\alpha\beta}^{z} c_{j\beta}, \\ H_{\mathrm{RSO}} &= i t_{\mathrm{R}} \sum_{\langle ij\rangle,\alpha\beta} c_{i\alpha}^{\dagger} \left(\boldsymbol{\sigma} \times \hat{\boldsymbol{d}}_{ij} \right)_{\alpha\beta}^{z} c_{j\beta}, \\ H_{\mathrm{m}} &= M \sum_{i,\alpha\beta} c_{i\alpha}^{\dagger} \sigma_{\alpha\beta}^{z} c_{i\beta}. \end{aligned}$$

The first term H_{hop} represents the nearest neighbor hopping term with hopping energy t, which is used as the energy unit in the following. The second term H_{ISO} is the intrinsic SOC involving the next-nearest neighbor hopping with amplitude t_{I}, $\nu_{ij} = \boldsymbol{d}_{kj} \times \boldsymbol{d}_{ik} / |\boldsymbol{d}_{kj} \times \boldsymbol{d}_{ik}| = \pm 1$, where $\boldsymbol{d}_{lm}$ is the vector along the bond from site m to a nearest site l. $\boldsymbol{\sigma} = (\sigma_x, \sigma_y, \sigma_z)$ is the vector of spin Pauli matrices. The summation over $\langle \ldots \rangle$ ($\langle\langle \ldots \rangle\rangle$) runs over all the nearest (next-nearest) neighbor sites. The third term H_{RSO} is the Rashba SOC with strength t_{R}, and $\hat{\boldsymbol{d}}_{lm} = \boldsymbol{d}_{lm} / |\boldsymbol{d}_{lm}|$ is a unit vector. The last term H_{m} represents a spin-splitting from a Zeeman-like coupling with strength M, which can be induced e.g. by the magnetic proximity effect.

The intrinsic SOC is from the crystalline structure of the honeycomb lattice. For graphene with a flat planar structure, its value is small because it is a second order process. For a low-buckling structure in which A and B sites have a relative shift in the out-of-plane direction, the intrinsic SOC can be greatly enhanced, as in silicene and germanene. Recently, large intrinsic SOC has been predicted for Bi/Sb hydrides and halides because of the p_x and p_y orbital character of the low energy bands in these materials [26, 27]. The Rashba SOC generally results from the structural inversion asymmetry along the out-of-plane direction, which may be induced by a substrate, atom adsorption, or an external electric field along the z-direction.

Here we emphasize that our main objective in this paper is to explore new topological states of matter. Hence we are trying to take a model which is as simple as possible but still supports the desired topological states, and we are not aiming to analyze any comprehensive

models for existing real materials[6]. In general, there are many possible symmetry-allowed SOC terms when far-neighbor intralayer and interlayer hopping processes are considered, e.g. as being studied for the case of bilayer graphene [36, 37]. Here we disregard the far-neighboring hopping processes and assume that the interlayer coupling is weak. Therefore, we only retain the two intralayer SOC terms (the intrinsic SOC and the Rashba SOC) in the model which are needed for realizing the interesting topological metallic phases we discuss below.

As a comment on the symmetry property of our model, we observe that when $U = M = 0$ the system has both inversion symmetry and time reversal symmetry: the system is a zero gap semiconductor. A finite U breaks inversion symmetry, while a finite M breaks time reversal symmetry, leading to symmetry-breaking ground states. This generally opens a bulk gap. In the following, we shall analyze these symmetry-breaking states in detail.

3. $\mathbb{Z}_2$-metallic phase

We first consider the case with preserved time reversal symmetry by setting $M = 0$. In this case, the Chern invariant must vanish. However, the system can still have a nontrivial $\mathbb{Z}_2$ invariant. If the system has preserved spin component, e.g. with only intrinsic SOC and vanishing Rashba SOC, the two spin species have opposite Chern numbers. Then the $\mathbb{Z}_2$ invariant is just equal to (half) the difference between the Chern numbers of the two spin species $\sigma_z = \pm 1$ (modular 2). For the general case with no conserved spin components, the $\mathbb{Z}_2$ invariant can be computed using the following formula [38, 39]:

$$\mathbb{Z}_2 = \frac{1}{2\pi}\left[\oint_{\partial \mathrm{HBZ}} \mathrm{d}\boldsymbol{k} \cdot \boldsymbol{A}(\boldsymbol{k}) - \int_{\mathrm{HBZ}} \mathrm{d}^2k \; \Omega_z(\boldsymbol{k}) \right] \mathrm{mod}\ 2, \tag{3}$$

where $\boldsymbol{A}(\boldsymbol{k}) = i\sum_n \langle u_n(\boldsymbol{k}) | \nabla_k u_n(\boldsymbol{k}) \rangle$ is the Berry connection summed over all the occupied bands, $|u_n(\boldsymbol{k})\rangle$ is the periodic part of the Bloch state for band n. $\Omega_z(\boldsymbol{k}) = (\nabla_k \times \boldsymbol{A})_z$ is the z-component of the Berry curvature. HBZ denotes half of the Brillouin zone, and the line integral is along the boundary of the HBZ. In this approach, the following constraint needs to be imposed on the wave function for the line integral: $|u_n(-\boldsymbol{k})\rangle = \Theta |u_n(\boldsymbol{k})\rangle$, where Θ is the time reversal operator. The $\mathbb{Z}_2 = 1$ state is topologically distinct from the $\mathbb{Z}_2 = 0$ state, in that they cannot be adiabatically connected to each other (through tuning some system parameter) without closing the bulk gap. The $\mathbb{Z}_2 = 0$ state is connected to the trivial vacuum, hence is the trivial insulating state. The $\mathbb{Z}_2 = 1$ state is nontrivial, and is known as the QSH state. It has an odd number of Kramers pairs of helical edge channels that are protected by time reversal symmetry.

It has been shown that the single layer Kane–Mele model with only intrinsic SOC is a $\mathbb{Z}_2 = 1$ QSH ground state. This phase persists with finite Rashba SOC as long as the bulk gap does not close. With further increasing Rashba SOC, the gap finally closes and the QSH phase is destroyed. For a bilayer Kane–Mele model with each layer being a $\mathbb{Z}_2 = 1$ insulator, the combined system is in fact trivial because $1 + 1 = 0$ (mod 2). The case of a bilayer model with

[6] In this work, although we are not particularly concerned with specific materials for realizing the bilayer Kane–Mele model, nevertheless we point out that, given the single layer Kane–Mele model could be achieved (e.g. in Bi/Sb hydrides or halides), it is likely to realize the bilayer model by combining two such layers and engineering the structure to achieve the desired weak coupling between them.

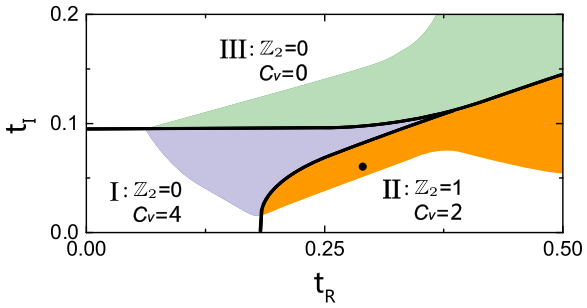

Figure 2. Phase diagram of the bilayer Kane–Mele model as a function of t_{R} and t_{I}. The solid lines separate three phases with different topological invariants $\mathbb{Z}_2$ and C_{v}. The colored regions are the metallic states where the band gap closes indirectly. The parameters used here are $t = 1$, $U = 0.5$, $M = 0$, and $t_{\perp} = 0.2$.

only Rashba SOC has been studied before [35]. It has been found that under finite interlayer potential U the Rashba SOC in fact helps to realize a QSH state.

When the intrinsic SOC comes into the play, from the previous discussion one expects that it tends to drive the system into the trivial phase, hence it has a competition with the Rashba SOC in the topological phase transition. Here we calculate the topological phase diagram reflecting the competition between the two SOCs. The result is shown in figure 2 as functions of t_{R} and t_{I}. The boundary between different topological phases corresponds to the states where the conduction band and the valence band touch. The black lines in the diagram mark such band-touching states. Here a finite interlayer potential U is taken to open a bulk gap initially and its relevance to the topological metallic states will be discussed in a while. We observe that the phase diagram is divided by the band-touching lines into three regions. As expected, for large t_{I}, when the intrinsic SOC dominates over the Rashba SOC, the system takes a $\mathbb{Z}_2 = 0$ trivial phase (the upper part labeled as region III). For the opposite case, when the Rashba SOC dominates over the intrinsic SOC for large t_{R}, the system takes a $\mathbb{Z}_2 = 1$ QSH phase (the lower right part labeled as regi on II). One notes that the band-touching lines separate out another region at the lower left corner (region I) when both t_{I} and t_{R} are small, which also has $\mathbb{Z}_2 = 0$. Although both I and III are trivial in terms of $\mathbb{Z}_2$ classification, region I differs from III in the valley Chern number. Strictly speaking, the Chern invariant (number) is defined only for a closed manifold [9, 40],

$$C = \frac{1}{2\pi}\sum_{n}\int \mathrm{d}^2k\ \Omega_z(\boldsymbol{k}), \tag{4}$$

where the integral is usually over the Brillouin zone. Because Berry curvature is odd under time reversal, the total Chern number must vanish in our present case. For a honeycomb lattice, the Brillouin zone has a hexagon shape and the energy spectrum has two valleys K and K′ at the corners of the Brillouin zone, where the Berry curvature Ω_z is concentrated. In figure 3(b), we plot a typical Berry curvature distribution in k-space. One observes that the curvature is peaked around the valleys, and it has different signs between the K and K′ valleys. Therefore, one can define a valley Chern number C_{v} as the difference between the integrals of the Berry curvature around the two valleys. For the three regions in figure 2, we have $C_{\mathrm{v}} = 4$ for region I, $C_{\mathrm{v}} = 2$ for region II, and $C_{\mathrm{v}} = 0$ for region III. The valley Chern number physically determines the

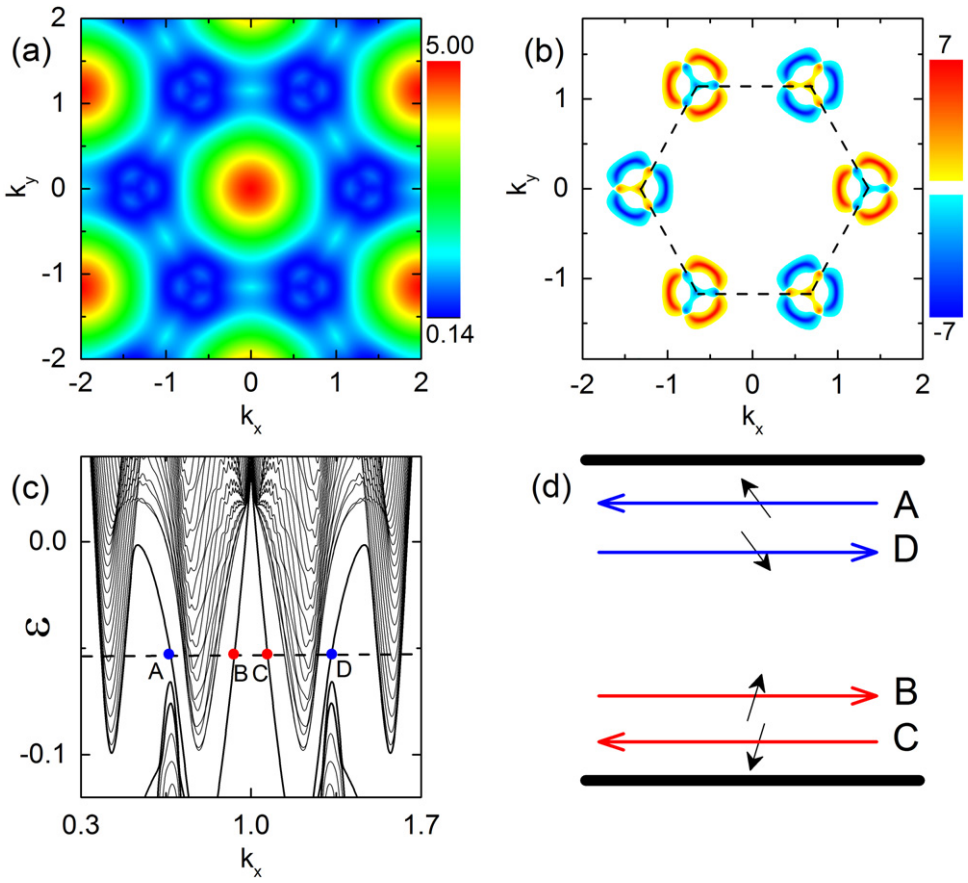

Figure 3. (a) Map of direct energy gap in k-space, (b) Berry curvature distribution in the Brillouin zone, and (c) the spectrum of a zigzag-terminated ribbon for a typical $\mathbb{Z}_2$-metallic state corresponding to the marked point in the phase diagram figure 2 with $t_R = 0.3$ and $t_I = 0.06$. The colored points in (c) label the edge modes localized at opposite boundaries, as schematically shown in (d) along with their spin polarizations.

quantum valley Hall (QVH) conductance of the system [41–44]. Hence, region I corresponds to a QVH phase while region III is valley Hall trivial.

What is more interesting about the present system is that we find there are extended regions around the phase boundaries in which the states are in fact metallic. The global bulk gap closes in the colored regions in figure 2. Because a metal does not have a stable ground state against excitations, usually it does not permit a topological phase. At first sight, one might guess that the colored area in region II is just a trivial metallic phase, for which a topological invariant cannot be defined. However, we find that, although these states do not have a global bulk gap, they do have a local bulk gap at every k-point in the Brillouin zone. In figure 3(a), we plot the map of the local direct gap of such a metallic state. It shows that the local gap is always bigger than zero. This means that the valence bands are still well separated from the conduction bands and form an isolated manifold. They are adiabatically connected to the insulating state in each region without closing the local bulk gap (band-touching), hence also share the corresponding topological invariants.

We are most interested in the metallic states in region II. From the above argument, the metallic states there should have $\mathbb{Z}_2 = 1$ with spin helical edge channels, representing a 2D $\mathbb{Z}_2$

-metallic phase. In figure 3(c), we show the energy spectrum calculated for a zigzag-terminated ribbon of the system, corresponding to the marked point in the phase diagram. We observe that the band gap closes indirectly and there are edge states connecting the conduction band and the valence band. Note that the topological property is a bulk property, which does not depend on the edge termination. The helical edge states are present also for armchair and any other types of edge. We analyze the spatial distribution and spin polarization of these edge states. The result is plotted schematically in figure 3(d). From this figure, we can clearly observe that on each edge there is one Kramers pair of spin helical edge states, as dictated by the $\mathbb{Z}_2 = 1$ requirement. As long as the time reversal symmetry is preserved, the two states on the same edge cannot be mixed with each other. Because of the absence of a global band gap, these edge states coexist at the same energy as bulk bands, hence they are not as robust as the edge states for QSH insulators. However, since they do not overlap with the bulk bands in momentum, they could still remain a sharp state against smooth scattering potentials.

Such a $\mathbb{Z}_2$-metallic state is analogous to the 3D Sb crystal. It has been found that the band gap of Sb also closes indirectly and its ground state has a nontrivial 3D $\mathbb{Z}_2$ invariant [45]. Recent experiments on the 3D [Tl]MTe family also found similar phenomena [46]. There are two differences. One is that the current $\mathbb{Z}_2$-metallic state is realized in a 2D system. The other one is its emergence here is a result of the competition between two types of SOC. As observed from the phase diagram, it requires both t_I and t_R to have finite values. The unique feature of this $\mathbb{Z}_2$-metallic state is the existence of topologically spin helical edge channels along with a metallic bulk.

We also mention that the coexistence of spin helical edge states and the bulk bands at the same energy could in fact be advantageous for engineering topological superconductivity. For example, analogous to the proposal for the 3D case [47], if the bulk of a 2D $\mathbb{Z}_2$-metal could form a conventional s-wave superconductor then the induced pairing in spin helical channels would turn the edge into an effective 1D p + ip superconductor [48].

Similar arguments apply to the metallic states in region I and region III as well. These metallic states also maintain a local gap across the Brillouin zone. They are adiabatically connected to the corresponding insulating states in each region, and hence share the topological properties of these insulating states. Therefore, the colored area in region III is a trivial metallic phase, while the colored region in region I is a QVH metallic phase.

In the calculation of the phase diagram (figure 2), we set a finite layer bias potential U. We mention that, although there is no topological insulator phase (i.e. with a global bulk gap) when $U = 0$ in this bilayer model [32–34], our $\mathbb{Z}_2$ topological metal phase still exists. In this case, the phase-I ($\mathbb{Z}_2 = 0$, $C_v = 4$) disappears, which is consistent with previous results [35]. However, the $\mathbb{Z}_2$-metallic states still exist with local gaps due to the competition between the two SOCs. The resulting $\mathbb{Z}_2$-metallic state is similar to the topological semiconducting state recently found in a single layer Kane–Mele–Hubbard model [50]. Therefore, the layer bias potential U is not necessary for realizing the $\mathbb{Z}_2$-metallic state. Here we choose to include a finite U because the local gaps in the topological metal states could be more clearly observed. The adiabatic transition between the $\mathbb{Z}_2$-metallic state and topological insulator state also makes the topological nature of these metallic states more obvious. Furthermore, a richer phase diagram can be generated, with the QVH phase and with the inclusion of topological invariant C_v. Different phases are distinguished by both topological invariants $\mathbb{Z}_2$ and C_v. The $\mathbb{Z}_2$-metal phase here has both $\mathbb{Z}_2$ invariant and C_v invariant. Therefore, the $\mathbb{Z}_2$-metallic state is protected by both time-reversal symmetry ($\mathbb{Z}_2 = 1$) and valley separation ($C_v = 2$). This novelty of the

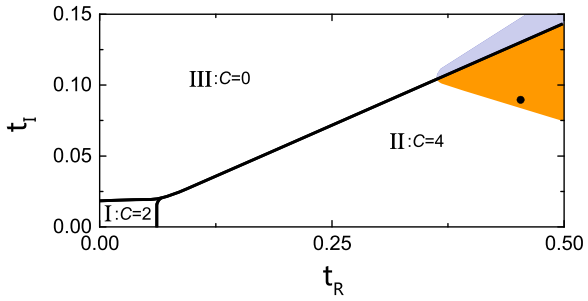

Figure 4. Phase diagram for the bilayer Kane–Mele model with time reversal symmetry breaking. The solid lines separate three phases with different Chern numbers C. The dot marks a Chern metallic state. The parameters used for the calculations are $t = 1$, $M = 0.1$, $U = 0$, and $t_\perp = 0.2$.

topological protection from valley separation has not yet been mentioned, e.g. in the study of the single-layer Kane–Mele model [49, 50]. This newly discovered $\mathbb{Z}_2$ topological metallic state hence exhibits features of both QSH and QVH systems.

4. Chern metallic phase

When time reversal symmetry is broken, the topological classification of a 2D insulator changes from $\mathbb{Z}_2$ to $\mathbb{Z}$, characterized by the Chern number. The Chern number, given by the integral of Berry curvature over the entire Brillouin zone, determines the number of chiral edge channels of the system. For our bilayer Kane–Mele model, the time reversal symmetry is broken by a finite M value, which generates a Zeeman spin-splitting. This term is introduced on a mean field level and could be physically induced by magnetic dopants or the proximity effect from nearby magnetic layers. [6] Here we set $U = 0$ so that the system preserves inversion symmetry. Following the same methodology as in the previous section, we calculate the phase diagram with respect to the parameters t_R and t_I. In figure 4, the phase boundaries, which are the band-touching lines, separate the phase diagram into three regions. Region I in the lower left corner with both t_I and t_R small is an insulating phase with Chern number $C = 2$. In region II, t_R dominates over t_I, and we have $C = 4$. This is consistent with the previous observation that $C = 2$ for a single layer with only Rashba SOC. In region III, t_I dominates over t_R, and we have $C = 0$, indicating that it is a trivial phase.

If we analyze the spectrum of the system, we find that there are also extended areas in region II and region III for which the global gap closes but a local direct gap is still maintained. This is demonstrated in figure 5(a) for a typical case, in which one observes that the direct gap is always positive throughout the Brillouin zone. Due to the presence of the local gap, the valence bands are separated from the conduction bands. These metallic states are adiabatically connected to the insulating states in the same region. The metallic states in region III are trivial, while the metallic states in region II are topologically nontrivial.

Let us focus on the states in region II, which has a Chern number $C = 4$. The adiabatic connectivity means that the metallic state shares the same topological character as the Chern insulator state: it also has chiral edge states and a Chern number can be defined for its valence bands with $C = 4$. We shall call these novel states Chern metals.

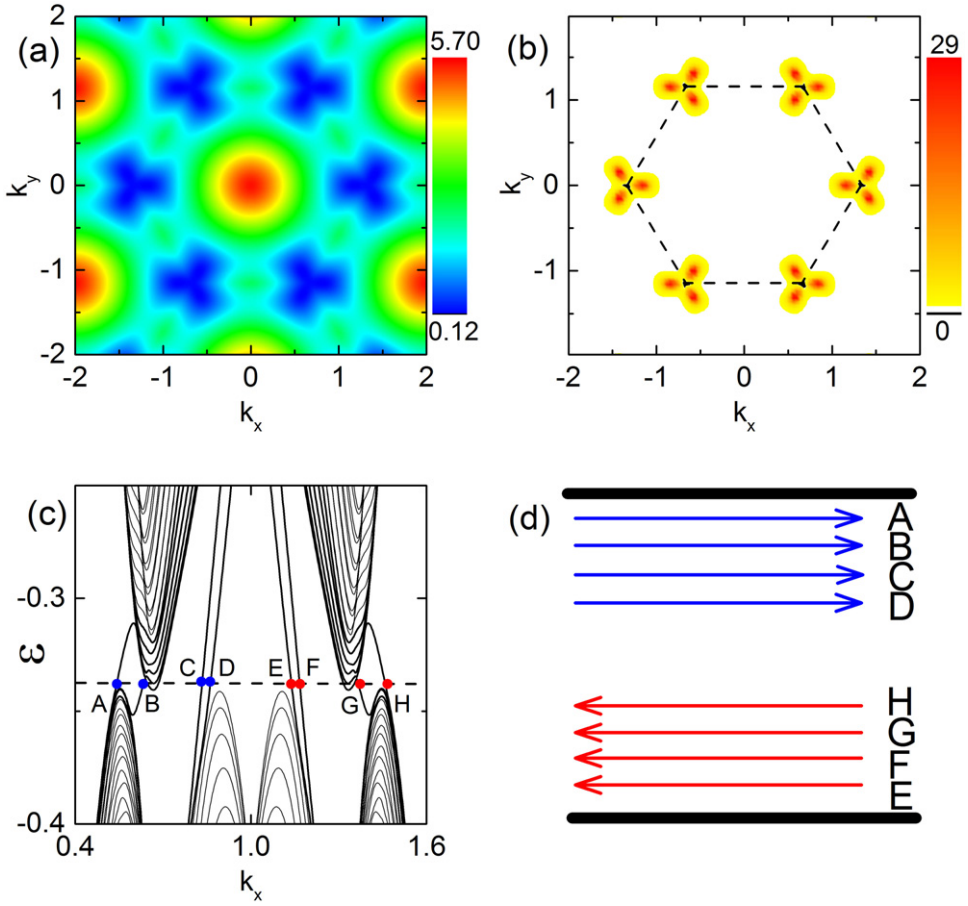

Figure 5. (a) Direct energy gap, (b) Berry curvature distribution in the Brillouin zone, and (c) the spectrum of a zigzag-terminated ribbon for a typical Chern metallic state as marked in the phase diagram figure 4 with $t_R = 0.45$ and $t_I = 0.09$. The colored points in (c) label the edge modes localized at opposite boundaries, as shown schematically in (d).

In figure 5(b), we show the Berry curvature distribution in k-space for the C metallic state marked by the dot in the phase diagram. It is observed that the Berry curvature is concentrated in each valley, and it has the same sign for different valleys, obeying the requirement from inversion symmetry. In figure 5(c), we plot the energy spectrum of a ribbon geometry for the Chern metallic state. We observe that the global bulk gap closes indirectly but the chiral edge states still exist. We analyze the spatial distribution of these edge states and the result is shown schematically in figure 5(d). On each edge, there are four channels propagating along the same direction, as required by the Chern number $\mathcal{C} = 4$. The existence of chiral edge channels along with a conducting bulk is the hallmark of this novel Chern metallic phase. Again because it is a metallic state, the chiral edge states are not as robust as those in an insulating state. However, since these edge states do not overlay with the bulk bands in momentum, they could still remain sharp states against smooth disorder potentials. From the phase diagram figure 4, we see that its appearance must require both t_{R} and t_{I} to have a finite value. Hence, like the $\mathbb{Z}_2$-metallic state, it is a result of the competition between the intrinsic SOC and the Rashba SOC.

5. Summary

In this work, we have studied the topological phases of a bilayer Kane–Mele model in detail. We find that the system exhibits a rich phase diagram as a result of the competition between the intrinsic SOC and the Rashba SOC. In contrast to the single layer case, there emerge novel 2D topological metallic phases that can be adiabatically connected to their topological insulator counterparts. In the presence of time reversal symmetry, we find there is a $\mathbb{Z}_2$-metallic phase with nontrivial $\mathbb{Z}_2$ invariant and spin helical edge states. When time reversal symmetry is broken, there exists a Chern metallic phase with nontrivial Chern invariant and chiral edge states. These findings broaden our knowledge of the topological states of matter. This also shows that, by controlling the competition between different SOCs, one can tune the topological phase and control both the bulk and edge conduction, which could be useful in applications based on topological materials.

Acknowledgments

The authors thank Fan Zhang, C-Y Zhang, and D L Deng for helpful discussions. This work was supported by SUTD-SRGEPD2013062, the MOST Project of China (grant nos 2014CB920903 and 2011CBA00100), the NSFC (grant nos 11174022, 61227902, 11174337, and 11225418), the NCET program of MOE (grant no. NCET-11-0774), and the Specialized Research Fund for the Doctoral Program of Higher Education of China (grant no. 20121101110046). ZQ is grateful for financial support from the 100 Talents Program of CAS and NNSFC (11034006).

References

[1] Hasan M Z and Kane C L 2010 *Rev. Mod. Phys.* **82** 3045
[2] Qi X L and Zhang S C 2011 *Rev. Mod. Phys.* **83** 1057
[3] Onoda M and Nagaosa N 2003 *Phys. Rev. Lett.* **90** 206601
[4] Yu R *et al* 2010 *Science* **329** 61
[5] Nagaosa N, Sinova J, Onoda S, MacDonald A H and Ong N P 2010 *Rev. Mod. Phys.* **82** 1539
[6] Qiao Z, Yang S A, Feng W, Tse W K, Ding J, Yao Y, Wang J and Niu Q 2010 *Phys. Rev.* B **82** 161414(R)
Ding J, Qiao Z H, Feng W X, Yao Y G and Niu Q 2011 *Phys. Rev.* B **84** 195444
[7] Tse W K, Qiao Z H, Yao Y G, MacDonald A H and Niu Q 2011 *Phys. Rev.* B **83** 155447
[8] Laughlin R B 1981 *Phys. Rev.* B **23** 5632
Halperin B I 1982 *Phys. Rev.* B **25** 2185
[9] Thouless D J, Kohmoto M, Nightingale M P and den Nijs M 1982 *Phys. Rev. Lett.* **49** 405
[10] Bernevig B A, Hughes T L and Zhang S C 2006 *Science* **314** 1757
[11] König M, Wiedmann S, Brune C, Roth A, Buhmann H, Molenkamp L W, Qi X L and Zhang S C 2007 *Science* **318** 766
[12] Liu C X, Hughes T L, Qi X L, Wang K and Zhang S C 2008 *Phys. Rev. Lett.* **100** 236601
[13] Knez I, Du R R and Sullivan G 2011 *Phys. Rev. Lett.* **107** 136603
[14] Knez I, Du R R and Sullivan G 2012 *Phys. Rev. Lett.* **109** 186603
[15] Chang C *et al* 2013 *Science* **340** 167
[16] Kane C L and Mele E J 2005 *Phys. Rev. Lett.* **95** 146802
Kane C L and Mele E J 2005 *Phys. Rev. Lett.* **95** 226801
[17] Yao Y, Ye F, Qi X L, Zhang S C and Fang Z 2007 *Phys. Rev.* B **75** 041401(R)

[18] Huertas-Hernando D, Guinea F and Brataas A 2006 *Phys. Rev.* B **74** 155426
[19] Min H, Hill J E, Sinitsyn N A, Sahu B R, Kleinman L and MacDonald A H 2006 *Phys. Rev.* B **74** 165310
[20] Lalmi B, Oughaddou H, Enriquez H, Kara A, Vizzini S, Ealet B and Aufray B 2010 *Appl. Phys. Lett.* **97** 223109
[21] Vogt P, Padova P D, Quaresima1 C, Avila J, Frantzeskakis E, Asensio M C, Resta A, Ealet B and Lay G L 2012 *Phys. Rev. Lett.* **108** 155501
[22] Fleurence A, Friedlein R, Ozaki T, Kawai H, Wang Y and Yamada-Takamura Y 2012 *Phys. Rev. Lett.* **108** 245501
[23] Chen L, Liu C C, Feng B, He X, Cheng P, Ding Z, Meng S, Yao Y and Wu K 2012 *Phys. Rev. Lett.* **109** 056804
[24] Tsai W F, Huang C Y, Chang T R, Lin H, Jeng H T and Bansil A 2013 *Nat. Commun.* **4** 1500
[25] Liu C C, Feng W and Yao Y 2011 *Phys. Rev. Lett.* **107** 076802
[26] Song Z, Liu C C, Yang J, Han J, Ye M, Fu B, Yang Y, Niu Q, Lu J and Yao Y 2014 arXiv:1402.2399
[27] Liu C C, Guan S, Song Z, Yang S A, Yang J and Yao Y 2014 *Phys. Rev.* B **90** 085431
[28] McCann E and Fal'ko V I 2006 *Phys. Rev. Lett.* **96** 086805
Koshino M and McCann E 2009 *Phys. Rev.* B **80** 165409
[29] Zhang F, Sahu B, Min H and MacDonald A H 2010 *Phys. Rev.* B **82** 035409
Zhang F, Jung J, Fiete G A, Niu Q and MacDonald A H 2011 *Phys. Rev. Lett.* **106** 156801
[30] Jung J, Zhang F, Qiao Z and MacDonald A H 2011 *Phys. Rev.* B **84** 075418
Qiao Z, Jung J, Niu Q and MacDonald A H 2011 *Nano Lett.* **11** 3453
Jung J, Qiao Z, Niu Q and MacDonald A H 2012 *Nano Lett.* **12** 2936
[31] Martin I, Blanter Ya M and Morpurgo A F 2008 *Phys. Rev. Lett.* **100** 036804
[32] Cortijo A, Grushin A G and Vozmediano M A H 2010 *Phys. Rev.* B **82** 195438
[33] Prada E, San-Jose Brey P L and Fertig H A 2011 *Solid State Commun.* **151** 1075
[34] Carmier P, Shevtsov O, Groth C and Waintal X 2013 *J. Comput. Electron* **12** 175
[35] Qiao Z, Tse W K, Jiang H, Yao Y and Niu Q 2011 *Phys. Rev. Lett.* **107** 256801
[36] Guinea F 2010 *New J. Phys.* **12** 083063
[37] Konschuh S, Gmitra M, Kochan D and Fabian J 2012 *Phys. Rev.* B **85** 115423
[38] Fu L and Kane C L 2006 *Phys. Rev.* B **74** 195312
[39] Fukui T and Hatsugai Y 2007 *J. Phys. Soc. Japan* **76** 053702
Essin A M and Moore J E 2007 *Phys. Rev.* B **76** 165307
[40] Xiao D, Chang M C and Niu Q 2010 *Rev. Mod. Phys.* **82** 1959
[41] Xiao D, Yao W and Niu Q 2007 *Phys. Rev. Lett.* **99** 236809
[42] Yao W, Xiao D and Niu Q 2008 *Phys. Rev.* B **77** 235406
[43] Yao W, Yang S A and Niu Q 2009 *Phys. Rev. Lett.* **102** 096801
[44] Pan H, Li Z, Liu C C, Zhu G, Qiao Z and Yao Y 2014 *Phys. Rev. Lett.* **112** 106802
[45] Fu L and Kane C L 2007 *Phys. Rev.* B **76** 045302
[46] Arpino K E *et al* 2014 *Phys. Rev. Lett.* **112** 017002
[47] Potter A C and Lee P A 2011 *Phys. Rev.* B **83** 184520
[48] Kitaev A Yu 2001 *Phys. Usp.* **44** 131
[49] Zhang F, Jung J and MacDonald A H 2011 *J. Phys.: Conf. Ser.* **334** 012002
[50] Laubach M, Reuther J, Thomale R and Rachel S arXiv: cond-mat/1312.2934